Title	Energy trapping of circumferential shear horizontal wave in a hollow cylinder
Author(s)	Iiboshi, Yuma; Iwata, Akito; Hayashi, Takahiro et al.
Citation	Ultrasonics. 2023, 133, p. 107044
Version Type	AM
URL	https://hdl.handle.net/11094/92341
rights	© 2023 Published by Elsevier B.V. This manuscript version is made available under the Creative Commons Attribution-NonCommercial-NoDerivatives 4.0 International License.
Note	

Energy trapping of circumferential shear horizontal wave in a hollow cylinder.

Yuma Iiboshi, Akito Iwata, Takahiro Hayashi, Naoki Mori
Graduate School of Engineering, Osaka University, Japan

Abstract
This paper describes energy trapping of circumferential shear horizontal wave (C-SH wave) at a circumferential inner groove of a hollow cylinder. We first derive exact solutions of resonant frequencies of the C-SH wave from the classical theory of guided waves propagating in a hollow cylinder and approximated solutions from the relationship between wavelength of the C-SH wave and length of circumferential path of the hollow cylinder. Next, we examined the energy trapping conditions using the dispersion curves of a guided wave propagating in the longitudinal direction of a hollow cylinder, and showed that C-SH waves trap energy when the hollow cylinder has a circumferential groove on the inner surface, rather than on the outer surface. The energy trapping at an inner groove was confirmed for the C-SH wave with the circumferential order of n= 6 using eigen frequency analysis of finite element method and experiments with electromagnetic transducers. Moreover, when the energy trap mode was used to determine the change in resonance frequency for glycerin solution of different concentrations, it was confirmed that the resonance frequency decreased monotonically as the concentration increased, indicating the possibility of using the energy trap mode as a QCM-like sensor.

Keywords: Energy trapping; Hollow cylinder; Circumferential shear horizontal wave; Resonance; Electromagnetic transducer;

1. Introduction

It has long been observed that the energy of elastic waves is confined in areas where the structure changes shape or where the material properties differ [1-8]. For example, a quartz crystal microbalance (QCM) has a thicker plate area at the electrodes on the piezoelectric plate, and the vibration energy input at the electrodes is trapped in the thick wall. Therefore, the QCM can achieve a stable resonance with a high Q value without being affected by the supports at a distance from the electrode. This means that the QCM has excellent properties as a sensor, and it is used as a highly sensitive sensor for small substances in liquid and gas by depositing a thin metal film that adsorbs the desired substance on the electrode area. When an antibody that adsorbs a specific protein is supported, it is used as a biosensor [9-12].

Many researches have been presented on energy trapping of guided waves propagating on curved surfaces. Johnson et. al. [13] showed the energy trapping of circumferential surface waves at a stepped circumferential band of a circular cylinder. Ogi et. al. developed a wireless and electrodeless biosensor using the energy trapping mode at the stepped circumferential band of a cylinder [14]. Yamanaka et. al. developed a gas sensor using the surface wave travelling around an equator of the sphere, which is also an energy-trapping mode on the equator [15, 16]. In the field of non-destructive testing, Fan and Lowe proposed detection of defects in weld lines using guided waves along the weld, which is also used the energy-trapping characteristic of guided waves in a weld line [17]. Furthermore, one of the authors of this paper discussed the energy trapping at a circumferential groove of a hollow cylinder where Lamb waves with the out-of-plain vibration form a standing wave in the circumferential direction, which was theoretically and experimentally examined in Ref. [18]. Although in-plane vibration generally has better performance as a sensor like the QCM, energy trapping of in-plane vibration in hollow cylinders has not been well studied.

This study investigates the energy trapping of circumferential shear horizontal wave (C-SH wave) at a circumferential groove in a hollow cylinder, aiming to the application to material evaluation and detection of micromaterials in a liquid and a gas. First, energy trapping conditions are theoretically and experimentally confirmed for the C-SH wave that has in-plane vibration and relatively small attenuation due to the leakage into the liquid. Moreover, we discuss its application to a sensing device from the experimental results of resonant frequencies in a hollow cylinder filled with various liquid with different viscosities.

2. Theory of energy trapping of circumferential shear horizontal wave in a hollow cylinder

This section describes principle of energy trapping of C-SH wave at a circumferential groove in a hollow cylinder. In Section 2.1, exact solution and approximated solution of resonant frequencies for the C-SH wave are obtained, and in Section 2.2, the principle of energy trapping of C-SH wave in an inner groove of a hollow cylinder is investigated using dispersion curves of guided waves propagating in the longitudinal direction.

2.1 Exact solution and approximated solution of resonant frequencies for the circumferential shear horizontal waves

Considering the shear horizontal wave propagating in the circumferential direction of a hollow cylinder with the inner and outer diameters of $2a$ and $2b$ and the transverse wave velocity of c_T, the resonant condition of the C-SH wave is given by the following equations, where the SH wave forms a standing wave in the circumferential direction with the nodes and antinodes of $2n$ [19-28].

$$\begin{vmatrix} c_{11} & c_{12} \\ c_{21} & c_{22} \end{vmatrix} = 0, \tag{1}$$

$$\begin{aligned} c_{11} &= \frac{n}{a} J_n(k_T a) - k_T J_{n+1}(k_T a), \\ c_{12} &= \frac{n}{a} Y_n(k_T a) - k_T Y_{n+1}(k_T a), \\ c_{11} &= \frac{n}{b} J_n(k_T b) - k_T J_{n+1}(k_T b), \\ c_{22} &= \frac{n}{b} Y_n(k_T b) - k_T Y_{n+1}(k_T b), \end{aligned} \tag{2}$$

where k_T is the wavenumber of transverse wave represented by $k_T = 2\pi f / c_T$ using vibration frequency f, and J_n and Y_n are Bessel functions of the first and second kind of the order of n. Then, the solutions of Eq. (1) with respect to the frequency f is the resonant frequencies of the C-SH wave in the hollow cylinder.

Since Eq. (1) is a nonlinear equation with respect to f, numerical methods are required to obtain the solutions. Therefore, noting that the C-SH wave exhibits almost the same vibration behaviour as SH plate waves propagating in a flat plate, the approximated resonant frequencies of the C-SH wave is obtained as follows. First, the fundamental SH plate wave has the wavelength of

$$\lambda = c_T / f\,. \tag{3}$$

If this wave propagates around a circumference of a hollow cylinder, the following phase matching condition becomes the resonant condition for the circumferential order of n.

$$2\pi r_0 = n\lambda\,, \tag{4}$$

where r_0 is the representative radius of the arc on which the C-SH wave propagates and the left side represents the propagation distance for one round. Reorganizing this in terms of frequency gives the resonant frequency for the n-th order mode as,

$$f_n = \frac{n c_T}{2\pi r_o}\,. \tag{5}$$

To estimate the approximated value of r_0, the resonant frequencies obtained by Eq. (5) are plotted in Fig. 2 for a nickel pipe used in the later experiments with the outer diameter of 10 mm and thickness of 0.5 mm, $a =$ 4.5 mm, $b =$ 5.0 mm, $c_T =$ 2970 m/s, assuming $r_o = a =$ 4.5 mm and $r_o = b =$ 5.0 mm in blue and red circles respectively, as well as the exact solutions of Eq. (1) in black dots. The exact values are located between the approximated values, which indicates that the approximated propagation path r_0 is between the outer and inner surfaces.

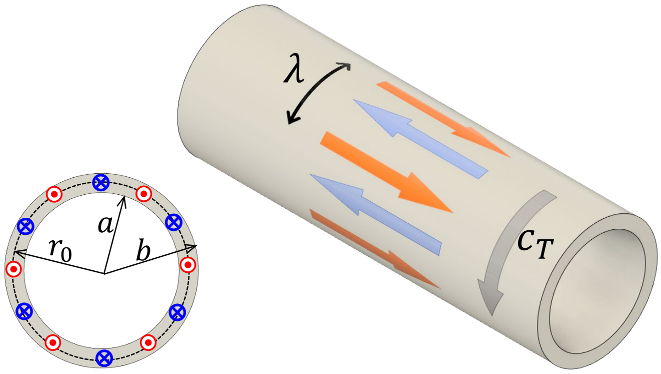

Fig. 1 Hollow cylinder and C-SH wave

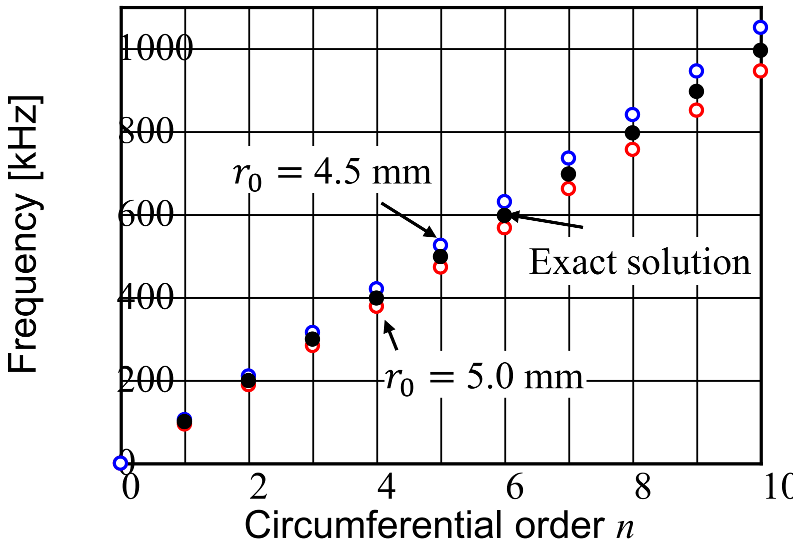

Fig. 2 Exact and approximated solutions of resonant frequencies of C-SH wave.

2.2 Prediction of energy trapping of the circumferential shear horizontal waves from dispersion curves

The resonant conditions of C-SH wave are obtained from Eq. (1) for exact solutions, and Eq. (5) for approximated solutions. When dynamic loading is applied by ultrasonic generation devices such as piezoelectric ultrasonic transducers, laser, and electromagnetic acoustic transducers (EMATs), the resonant standing wave can be formed, but it spreads in the longitudinal direction and diffuses throughout the pipe.

Therefore, this section discusses the energy trapping at a heteromorphic circumferential part with dispersion curves of guided waves propagating in the longitudinal direction. The black lines in Fig. 3 show dispersion curves of guided waves propagating in the longitudinal direction in a nickel hollow cylinder with an outer diameter of 10 mm, a thickness of 0.5 mm, and a transverse wave velocity c_T =2970 m/s. The horizontal and vertical axes are the wavenumber k and frequency f, respectively. The guided waves shown in the figure have the mode distribution of the circumferential order n = 6, meaning that they have $2n$ (=12) nodes and anti-nodes in the circumferential direction and propagate with the wavenumber of k in the longitudinal direction. It should be noted that the wavenumber has a real or pure imaginary number, the real and imaginary parts being represented in the right and left half of the graph. When the wavenumber is real, the wave distribution in the longitudinal (z) direction can be expressed as $\exp(ikz)$, showing the guided wave propagating in the z direction. On the vertical axis of k = 0, the wave shows the homogeneous distribution in the z direction and the circumferential order n = 6, indicating the standing wave of C-SH wave as discussed in Section 2.1. The frequency of the black line on the vertical axis of k = 0 is 597 kHz, which is the same value of the exact solution shown by the black dot at n = 6 in Fig. 2. In the frequency range below the cutoff frequency of 597 kHz, the wavenumber becomes a pure imaginary number (dashed line), showing the mode is evanescent in the longitudinal direction.

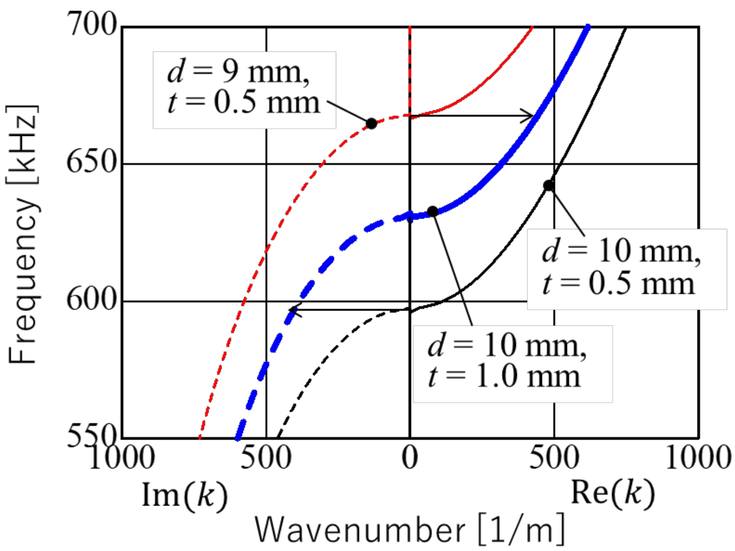

Fig. 3 Dispersion curves of guided waves propagating in the longitudinal direction of a nickel hollow cylinder for the circumferential order of n = 6.

The blue lines are dispersion curves of a nickel hollow cylinder for n = 6 with the same outer diameter as the black lines and the smaller thickness of 0.5 mm. And the red lines show ones with the outer diameter of 9.0 mm and the thickness of 0.5 mm. All curves are similar in shape, but shifted in the frequency direction.

Now we consider hollow cylinders with a circumferential stepped band as shown in Fig. 4; (a) has a groove on the outer surface of a pipe with the outer diameter of 10 mm, and (b) has a groove on the inner surface. The specimen in Fig. 4 (a) consists of two thick-walled pipes with the dispersion curves plotted with the blue lines of Fig. 3 and one thin pipe with the dispersion curves with the red lines between them, while the specimen in Fig. 4 (b) consists of the two thick-walled pipes with the blue curves and one thin pipe with the black curves. When the central groove in Fig. 4 (a) is subjected to vibration, a C-SH wave resonance occurs at the frequency of k = 0 in the red line (about 668 kHz). At the frequency, the pipes at both ends generate guided waves with a positive real number of wavenumbers k, as seen in the blue line in Fig. 3. That is, for the pipe combination in Fig. 4 (a), guided waves propagating in the longitudinal direction with the wave distribution of $\exp(ikz)$ are generated in both end pipes and energy is not trapped at the groove. On the other hand, for the pipe combination shown in Fig. 4 (b), when the groove is subjected to vibration, C-SH wave resonance occurs at the frequency position of k = 0 in the black line in Fig. 3 (about 597 kHz). In this case, the thick-walled pipes at the joints with the thin pipe generate vibration whose wavenumber k is a pure imaginary number, as shown by the blue lines in Fig. 3. Defining $k = ik'$ where k' is a real number, the longitudinally decaying vibration distribution is formed in the thick-walled pipes at the both joints, as $\exp(ikz) = \exp(-k'z)$. That is, when C-SH wave resonance occurs in the thin-walled center, vibration energy is trapped in and around the thin-walled part because the surrounding thick-walled part forms a vibration distribution that decays exponentially as the distance from the joint.

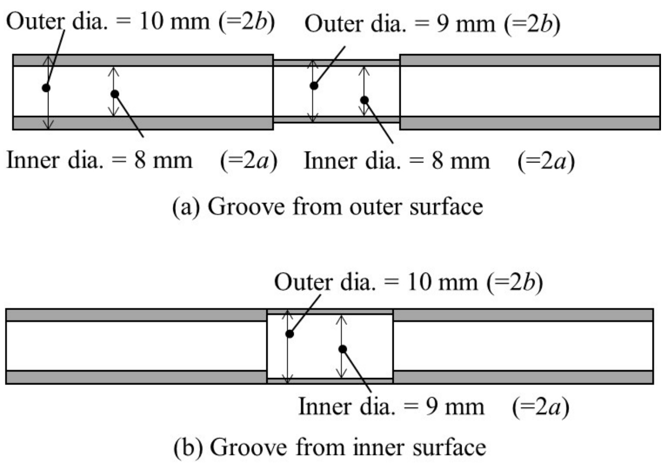

Fig. 4 Combinations of pipes with different wall thickness.

In other words, when considering trapping C-SH waves, it is necessary to use a pipe structure with an inner groove as shown in (b) instead of the outer groove as shown in (a).

3. Numerical validation of energy trapping of C-SH wave

In the previous section, the principle of energy trapping of C-SH wave at the resonant frequency of C-SH wave was discussed theoretically. However, those theories do not take into account the effects of mode conversion at the step and resonance of the entire structure, and it does not prove that they accurately represent actual energy trapping. In this section, we confirm the energy trapping of C-SH wave using the finite element method software COMSOL Multiphysics ®. Eigen frequency analysis was performed on the structure shown in Fig. 4 (b) to search for modes in which vibration energy is confined in the inner groove at the frequencies near the theoretical solution of the resonant frequency (597 kHz). The length of the inner groove region was set to 30 mm to correspond with later experiments, and the overall length was set to 170 mm. Traction-free boundary conditions were assumed for all surfaces. Figure 5 shows representative examples of the obtained resonance modes, with the surface color representing the longitudinal displacement. In (a) and (c), the vibrations are distributed outside of the central inner groove region, and are not the trapped modes of C-SH wave as considered here, but modes with the entire pipe resonance. On the other hand, (b) is the energy trapping mode, where the circumferential wave distribution matches well to n = 6, and vibration is confined only at the central grooved region, as predicted in Section 2.2. The frequency 599.3 kHz is about 2 kHz higher than the exact solution by Eq. (1) and the frequency at $k = 0$ in Fig. 3, 597 kHz. The differences between the exact solution of C-SH wave resonance and the eigen frequency of FE analysis are the junction of pipe step, the finite width of the groove, and the finite length of whole pipe, which causes the frequency difference.

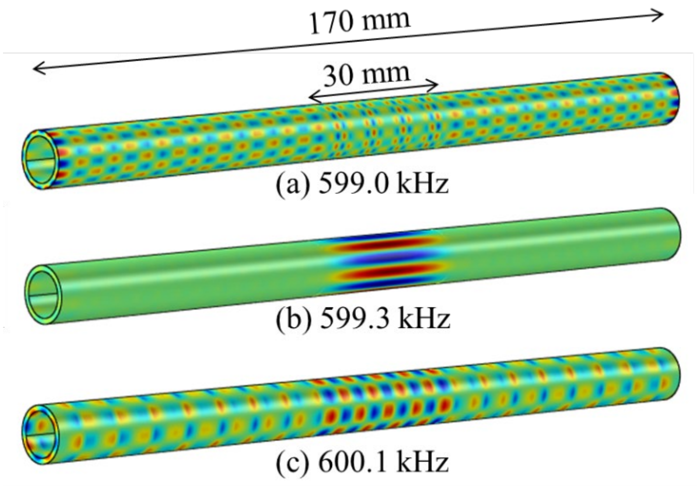

Fig. 5 Resonant modes around the resonant frequency for the C-SH wave of $n = 6$

4. Energy trapping experiments for an empty hollow cylinder

To experimentally confirm the energy trapping of C-SH waves, the resonance waveforms are measured using EMATs. A test pipe with an inner groove as shown in Fig. 4 (b) was made by gluing together a nickel pipe with an outer diameter of 10 mm, a wall thickness of 0.5 mm, and a length of 30 mm and two nickel pipes with an outer diameter of 10 mm, a wall thickness of 1.0 mm, and a length of 70 mm. The nickel test pipe generated the vibration with the magnetostriction occurred by a combination of static magnetic field from permanent magnets and dynamic magnetic field from a meandering coil placed along the wave distribution of $n = 6$, as shown in Fig. 6. The meandering coils were made from polyurethane enameled copper wire, and generation and detection coils were separately used in the experiments. A burst wave was applied to the meandering coil for excitation from a pulser receiver (RITEC RPR-4000), and the receiving signals were amplified 60 dB before an analog-digital converter (National Instruments, USB-5133). The digital data was processed in a personal computer, including filtering and Fourier transform. The signals were not averaged. A very large peak at 623 kHz was firstly observed when inputting burst signal of 600 kHz and 10 cycles to the meandering coil. Therefore, 623 kHz and 10-cycle burst signal was input in all experiments shown later. Figures 7 (a) and (b) are the receiving waveform and the frequency spectrum, respectively.

The frequency spectrum (b) was the Fourier transform of the waveform (a) after extracting the data from 50 μs to 500 μs and applying a Hamming window. In the frequency spectrum, in addition to a very large resonance peak at 623 kHz, small but distinct peaks appeared at 522 kHz and 727 kHz. In the approximate equation (5), when the physical quantity$c_T/2\pi r_o$, which consists of the material constant and pipe diameter, is set to 104 kHz, these peak frequencies approximately coincide with f_5, f_6 and f_7, and it can be concluded that these peaks are the C-SH wave resonances at $n =$ 5, 6, and 7. In this experimental system, the meandering coils were made to match the $n =$ 6 mode, but other modes may have appeared because the wires were bent by hand.

The resonant frequencies for $n =$ 5, 6, and 7 observed experimentally were shifted to the higher frequency by about 20 kHz (4 %) compared to the theoretical solutions in Fig. 2 and the numerical results in Fig. 5 (b). This is due to the material constants of the specimens being different from those used in the theoretical solutions and numerical calculations and slight errors in the pipe thickness, leading to the mismatch of $c_T/2\pi r_o$, and the difference may also be caused by the use of adhesive bonding to create the stepped sections of the specimens.

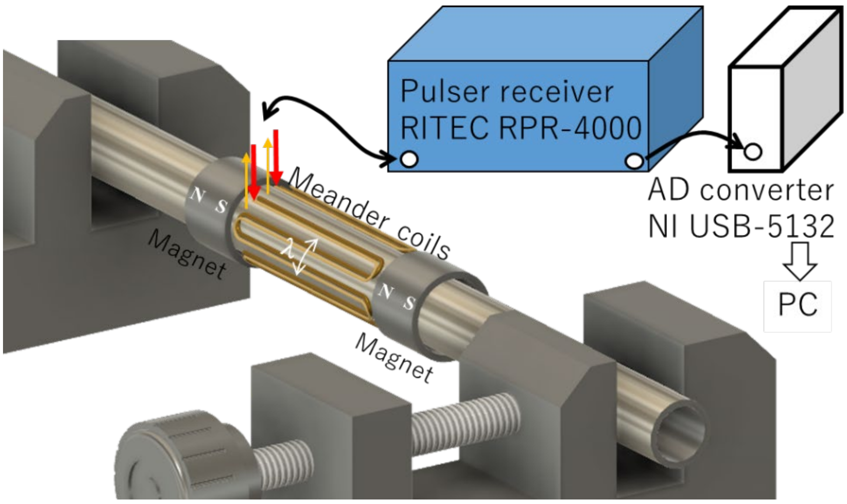

Fig. 6 Experimental set-up

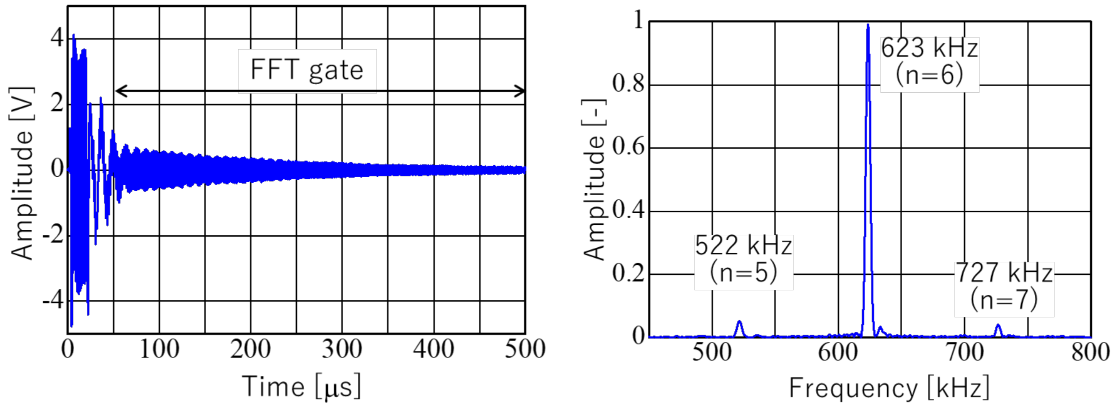

Fig. 7 Typical waveform and frequency spectrum

5. Measurement of resonant frequency change by contents

A QCM detects the presence of specific substances by measuring the resonance frequency, which varies with the mass and viscosity of the substance attached to the vibrating surface. For example, in biosensors, an antibody is loaded on a vibrating surface, and changes in resonant frequency due to specific proteins attached to the antibody are measured. In the hydrogen gas sensor, a hydrogen storage alloy such as a vanadium-based alloy that adsorbs hydrogen gas is attached to the vibrating surface and the resonance change is measured. In order to simply verify that the energy trapping of the in-plane vibration studied in this research can be used as a sensor, we confirm here that changes in resonance frequency can be measured by aqueous glycerin solutions of different concentrations.

As shown in Fig. 8, a tube for transporting aqueous solution and a pump were attached to both ends of the pipe specimen via adapters to enable the supply of aqueous solution into the test pipe. The waveform and frequency spectrum did not change at all when adapters were attached to both ends of the test pipe, indicating that the energy was properly trapped in the central groove. This property is also a major advantage of using the energy trapping as sensors. Frequency spectra were recorded using the measurement method described in Section 4.1 while the test pipe was filled with an aqueous solution. Waveform measurements were taken at a maximum concentration of 85%, followed by the addition of water, and the solution was thoroughly stirred and circulated to measure waveforms at the next concentration. Figure 9 shows the frequency spectra measured at 85, 80, 70, 60, 50, 40, 30, 20, 10, and 0 % by weight. The vertical axis of the peak position is normalized with respect to the amplitude value for the 0% (pure water) case. In addition, Fig. 10 plots the maximum value of this frequency spectrum (a) and the frequency at which it takes its maximum value (b). Measurements were taken twice. Figure 9 shows the results of the first measurement, and Fig. 10 shows all the results of two measurements. The peak value in Fig. 10 (a), which should be affected by ultrasonic attenuation, does not vary monotonically with concentration, but the peak frequency in (b) does. This change in peak frequency is consistent with the trend observed in QCMs, where the resonance frequency decreases with increasing viscosity of the material in contact with the surface in response to in-plane vibration, indicating that measurement of the resonance frequency of energy-trapped in-plane vibration at the inner groove can be used to evaluate the physical properties of the contents. In addition, a slight error in the peak frequency (b) was observed depending on the number of experiments, but this is considered to be due to slight temperature changes in the experimental environment and concentration errors in the solution.

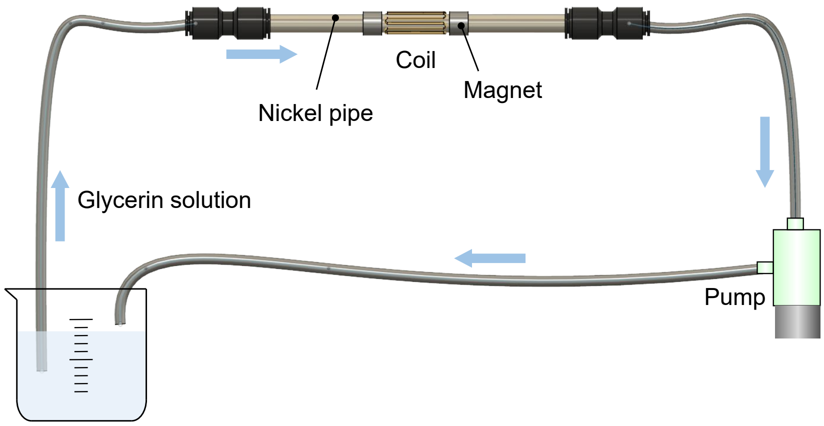

Fig. 8 Experimental system for measuring frequency change with concentration of glycerin solution

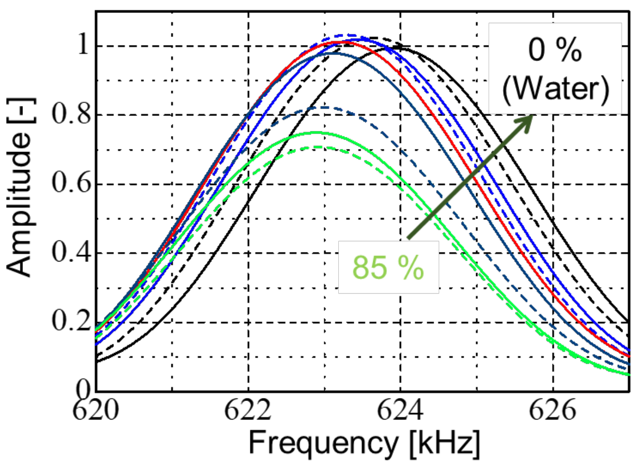

Fig. 9 Measured frequency spectra for various concentration of glycerin aqueous solution.

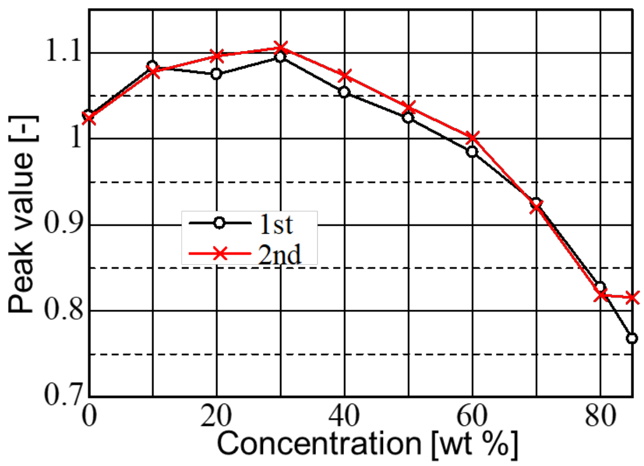

(a) Peak value

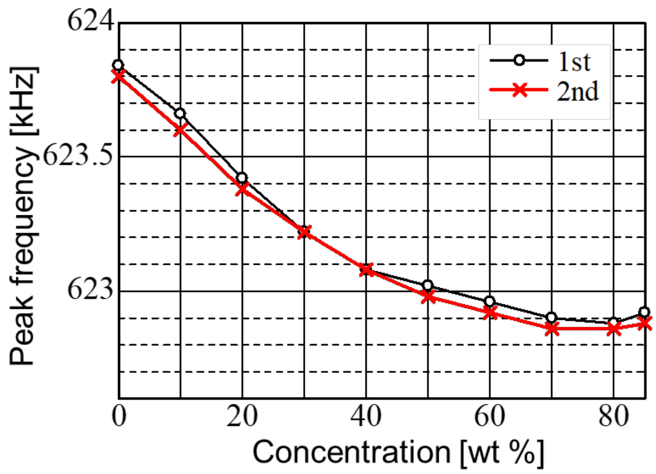

(b) Peak frequency

Fig. 10 Variation of measured values with concentration of glycerin solution

6. Summery

We theoretically investigated the conditions under which C-SH waves propagating in the circumferential direction of a hollow cylinder resonate as standing waves, and confirmed through numerical calculations and experiments that energy trapping of C-SH wave is observed in the circumferential grooves formed on the inner surface. Furthermore, as a basic experiment for utilizing this energy trapping phenomenon as a QCM-like sensor, changes in amplitude and resonance frequency were measured using aqueous solutions of glycerin of different concentrations. Although the amplitude did not show a monotonic change with concentration, the frequency showed a similar trend to that of the QCM, decreasing with increasing glycerol concentration.

Acknowledgement
The authors would like to thank Professor Hirotsugu Ogi for his insightful comments on QCMs and biosensors. This work was partially supported by JSPS KAKENHI Grant No.21H01573.

References

[1] W.H. King, Piezoelectric sorption detector, Anal Chem. 36 (1964) 1735–1739. https://doi.org/10.1021/ac60215a012.

[2] H. Watanabe, K. Nakamura, H. Shimizu, A new type of energy trapping caused by contributions from the complex branches of dispersion curves, IEEE Trans Sonics Ultrason. 28 (1981) 265–270. https://doi.org/10.1109/T-SU.1981.31257.

[3] K. Nakamura, Elastic wave energy-trapping and its application to piezoelectric devices, Electronics and Communications in Japan, Part II: Electronics (English Translation of Denshi Tsushin Gakkai Ronbunshi). 79 (1996) 30–39. https://doi.org/10.1002/ecjb.4420790704.

[4] M. Rodahl, B. Kasemo, On the measurement of thin liquid overlayers with the quartz-crystal microbalance, Sens Actuators A Phys. 54 (1996) 448–456. https://doi.org/10.1016/S0924-4247(97)80002-7.

[5] Z.T. Yang, S.H. Guo, Energy trapping in power transmission through a circular cylindrical elastic shell by finite piezoelectric transducers, Ultrasonics. 48 (2008) 716–723. https://doi.org/10.1016/j.ultras.2008.04.001.

[6] W. Wang, C. Zhang, Z. Zhang, T. Ma, G. Feng, Energy-trapping mode in lateral-field-excited acoustic wave devices, Appl Phys Lett. 94 (2009) 192901. https://doi.org/10.1063/1.3136853.

[7] H. He, J. Liu, J. Yang, Thickness-shear and thickness-twist vibrations of an AT-Cut quartz mesa resonator, IEEE Trans Ultrason Ferroelectr Freq Control. 58 (2011) 2050–2055. https://doi.org/10.1109/TUFFC.2011.2055.

[8] P. Li, F. Jin, J. Yang, Thickness-shear vibration of an AT-cut quartz resonator with a hyperbolic contour, IEEE Trans Ultrason Ferroelectr Freq Control. 59 (2012) 1006–1012. https://doi.org/10.1109/TUFFC.2012.2286.

[9] T. Nomura, M. Okuhara, Frequency shifts of piezoelectric quartz crystals immersed in organic liquids, Anal Chim Acta. 142 (1982) 281–284. https://doi.org/10.1016/S0003-2670(01)95290-0.

[10] K. Kanazawa, J. G. Gordon, The oscillation frequency of a quartz resonator in contact with liquid, Anal. Chim. Acta, 175 (1985) 99–105 https://doi.org/10.1016/S0003-2670(00)82721-X.

[11] M. Rodahl, B. Kasemo, Frequency and dissipation-factor responses to localized liquid deposits on a QCM electrode, Sens Actuators B Chem. 37 (1996) 111–116. https://doi.org/10.1016/S0925-4005(97)80077-9.

[12] H. Ogi, Wireless-electrodeless quartz-crystal-microbalance biosensors for studying interactions among biomolecules: A review, Proceedings of the Japan Academy, Series B. 89 (2013) 401–417. https://doi.org/10.2183/pjab.89.401.

[13] W. Johnson, B.A. Auld, E. Segal, F. Passarelli, Trapped torsional modes in solid cylinders, Journal of the Acoustical Society of America. 100 (1996) 285–293. https://doi.org/10.1121/1.415955.

[14] H. Ogi, K. Motohisa, T. Matsumoto, T. Mizugaki, M. Hirao, Wireless electrodeless piezomagnetic biosensor with an isolated nickel oscillator, Biosens Bioelectron. 21 (2006) 2001–2005. https://doi.org/10.1016/j.bios.2005.09.013.

[15] K. Yamanaka, S. Ishikawa, N. Nakaso, N. Takeda, Dong Youn Sim, T. Mihara, A. Mizukami, I. Satoh, S. Akao, Y. Tsukahara, Ultramultiple roundtrips of surface acoustic wave on sphere realizing innovation of gas sensors, IEEE Trans Ultrason Ferroelectr Freq Control. 53 (2006) 793–801. https://doi.org/10.1109/tuffc.2006.1621507.

[16] T. Tsuji, T. Oizumi, N. Takeda, S. Akao, Y. Tsukahara, K. Yamanaka, Temperature compensation of ball surface acoustic wave sensor by two-frequency measurement using undersampling, Jpn J Appl Phys. 54 (2015) 07HD13. https://doi.org/10.7567/JJAP.54.07HD13.

[17] Z. Fan, M. J. S. Lowe, Elastic waves guided by a welded joint in a plate, Proc. R. Soc. A Math. Phys. Eng. Sci., 465 (2009) 2053–2068. https://doi.org/10.1098/rspa.2009.0010

[18] T. Hayashi, Energy trapping of circumferential resonant modes at a thin-walled groove in a hollow cylinder, Journal of the Acoustical Society of America. 146 (2019). https://doi.org/10.1121/1.5129561.

[19] D. C. Gazis, Exact analysis of the plane-strain vibrations of thick-walled hollow cylinders, J. Acoust. Soc. Am., 31 (1959), 573–578 https://doi.org/10.1121/1.1909761.

[20] J. L. Rose, Ultrasonic Waves in Solid Media, Cambridge University Press, Cambridge, United Kingdom, 1999.

[21] K. F. Graff, Wave Motion in Elastic Solids, Dover Publications, New York, 1991.

[22] H. Nishino, R. Yokoyama, H. Kondo, K. Yoshida, Generation of circumferential guided waves using a bulk shear wave sensor and their mode identification, Japanese Journal of Applied Physics, Part 1 46 (2007) 4568–4576. https://doi.org/10.1143/JJAP.46.4568.

[23] G. Jie, L. Yan, Z. Mingfang, L. Mingkun, L. Hongye, W. Bin, H. Cunfu, Analysis of longitudinal guided wave propagation in the functionally graded hollow cylinder using state-vector formalism and Legendre polynomial hybrid approach, J Nondestr. Eval. 40 (2021). https://doi.org/10.1007/s10921-021-00764-y.

[24] X. Wang, F. Li, B. Zhang, J. Yu, X. Zhang, Wave propagation in thermoelastic inhomogeneous hollow cylinders by analytical integration orthogonal polynomial approach, Appl Math Model. 99 (2021) 57–80. https://doi.org/10.1016/J.APM.2021.06.008.

[25] X. Zhang, Z. Li, X. Wang, J. Yu, The fractional Kelvin-Voigt model for circumferential guided waves in a viscoelastic FGM hollow cylinder, Appl Math Model. 89 (2021) 299–313. https://doi.org/10.1016/J.APM.2020.06.077.

[26] H. Miao, F. Li, Shear horizontal wave transducers for structural health monitoring and nondestructive testing: A review, Ultrasonics. 114 (2021). https://doi.org/10.1016/j.ultras.2021.106355.

[27] A.C. Kubrusly, S. Dixon, Application of the reciprocity principle to evaluation of mode-converted scattered shear horizontal (SH) wavefields in tapered thinning plates, Ultrasonics. 117 (2021). https://doi.org/10.1016/j.ultras.2021.106544.

[28] J. Lin, J. Li, C. Jiang, X. Chen, Z. Tang, Z. Zeng, Y. Liu, Theoretical and experimental investigation of circumferential guided waves in orthotropic annuli, Ultrasonics. 123 (2022) 106715. https://doi.org/10.1016/J.ULTRAS.2022.106715.